Bio-Design and Manufacturing (2020) 3:109–121
https://doi.org/10.1007/s42242-020-00065-9

RESEARCH ARTICLE

Study on linear bio-structure print process based on alginate bio-ink in 3D bio-fabrication

Youping Gong[1] · Zhikai Bi[1] · Xiangjuan Bian[2] · Anlei Ge[1] · Jingyang He[1] · Wenxin Li[1] · Huifeng Shao[1] · Guojin Chen[1] · Xiang Zhang[3]

Received: 6 January 2020 / Accepted: 15 February 2020 / Published online: 10 March 2020

Abstract
Ink-jet printing is a non-impact printing technology in which drops jetted from an orifice onto a designated position. This technology can digitally transport fluids containing cells precisely onto desired substrates to construct three-dimensional organs. In order to obtain the stable uniform droplets, a stream is the key point of this technology. However, there are so many factors that affect the uniform droplet stream construction process: print parameters, material parameters, control method, etc. A good understanding of the various coupled transport processes that occur during bio-ink impact and spreading on bio-structure can improve the success of print-ability. This paper aims to obtain a good linear bio-structure with ink-jet printing technology. First, a typical droplet deposition process model is constructed; including droplet dynamics impact models and droplet diffusion cap models. Second, a model of successive droplet overlap, to form linear bio-structures, is constructed. Third, the finite element method is used to simulate the droplet impact, collision, and fusion process. Finally, the main influencing factors of the continuous injection printing process, namely the time interval between consecutive droplets and the droplet contact angles, are discussed. Sodium alginate is selected as bio-ink to verify the theory, and it is found that a good linear bio-structure could be obtained if the printing parameters are controlled optimally, i.e., if the initial contact angle is set as 60 degrees and the trigger frequency is set as 150 kHz. With a proper printing speed and gel coating, a good survival rate of printed cells could be obtained.

Keywords Sodium alginate · 3D Bio-fabrication · Drop-on-demand inject · Printing process simulation · Linear bio-structure

List of symbols

R_{droplet}	The radius of the initial droplet
R	The droplet spreading radius
r	The radius of the gap
h	The height of the cap
θ	The contact angle
θ_a	The contact angle when spreading to the maximum area
U_0	The dropping speed

✉ Xiangjuan Bian
bianxiangjuan@163.com

Youping Gong
gyp@hdu.edu.cn

Zhikai Bi
bzk1996@163.com

Anlei Ge
geanlei2020@163.com

Jingyang He
treasuresweet@163.com

Wenxin Li
Wwenxindiaolong@163.com

Huifeng Shao
shaohf@hdu.edu.cn

Guojin Chen
chenguojin@163.com

Xiang Zhang
zhangxiang@zzu.edu.cn

[1] School of Mechanical Engineering, Hangzhou Dianzi University, Hangzhou 310018, China

[2] Faculty of Science and Technology, Zhejiang International Studies University, Hangzhou, China

[3] National Center for International Joint Research of Micro-Nano Molding Technology, Zhengzhou University, Zhengzhou 450001, China

D_0	The diameter of the droplet
ρ	The density of fluid
σ	The surface tension
E_{K1}	The kinetic energy
E_{S1}	The surface energy of the droplet
E_{S2}	The surface energy of droplets falling on the substrate and spreading to the maximum area
W	The viscous dissipated energy
t_c	The spreading time
Ω	The volume of viscous fluid
φ	The dissipation function
δ	The thickness of the spreading boundary layer
Re	The Reynolds number of fluid
U_R	The droplet spreading speed
d	The spreading diameter of the base plate when the droplet impacts
D	The diameter of the wetted surface area
H	The thickness of liquid when spreading to maximum diameter
β	The original spread factor computation formula
β_{new}	The new spread factor computation formula
v	The nozzle moving speed
f	The transmission frequency
Δx	The center distance between the prints
L	The length of linear bio-structure
N	The droplet number of printed
r_e	The equilibrium wetting radius
U	The moving speed of the base plate
W_f	The maximum width of linear bio-structure

Introduction

In the traditional method of tissue engineering, a biomaterial scaffold is adapted to seed cells from a patient, and an organ construct is cultured via a bioreactor and then implanted into the patient [1]. A critical problem, however, exists. The patient cannot wait for too long to obtain the construct. The engineered tissue construct must control cells in three-dimensional (3D) spaces and assemble them as a functional structure. All the methods for 3D cellular patterning currently being researched have advantages and substantial disadvantages. The disadvantages of the old 3D cell fabrication methods have led researchers to recently focus on ink-jet printers [2, 3]. Ink-jet printing is a non-contact printing technique. By receiving data from a computer, ink-jet printers print tiny ink drops onto a substrate without hurting the cells. Ink-jet printers can either drop ink continuously or by the drop-on-demand (DoD) technique during which ink drops are printed only where and when they are required to create structures on the substrate. The ink stream is broken into equal-sized droplets by applying a piezoelectrically modulated pressure wave behind the nozzle. Ink-jet printing can accurately transfer liquid-containing cells to the required substrate to form a three-dimensional organ, which is a superior way to adapt to micro-droplet impact solid-surface printing in various coupling transmission processes.

Although ink-jet printing technology was in continuous use for many decades in the paper graphics industry, its application to nanotechnology-based fabrication processes presents many challenges. The physics of drop formation and detachment during ink-jet printing defines the range of ink fluid properties (surface tension, viscosity, volatility) for successful printability. The application of ink-jet printing in bio-fabrication requires the precise control of the final pattern and shape [4]. Such control demands a good understanding of the various coupled transport processes that occur during ink impact and spreading on a non-porous solid surface, coalescence with previously deposited fluid/dried structures, and the final assembly of the functional solid.

This study aims to investigate the fabrication process of 3D vascular-like tubular constructs using ink-jet printing. As illustrated in Fig. 1a, during ink-jetting, the 3D tubular construct could be printed vertically or horizontally based on the relative configuration between the moving direction of the dispensing nozzle and the axis of the tube being printed [5]. The typical horizontal printing setup is illustrated in Fig. 1b. The dispensing head, attached to the XY stages, travels parallel to the longitudinal axis of the tube at the designed velocity, and the alginate droplets are precisely positioned as the constituent elements to form a polygonal layer at the given height.

A z-shaped platform is used to improve the adhesion between the platform and the tube being printed. If the moving direction of the nozzle is parallel to the longitudinal axis of the tube, the fabrication process, as illustrated in Fig. 1c, is called horizontal printing. Horizontal printing technology could realize complex vascular network construction. The authors previously conducted detailed research on a method for predicting the compensation path during the printing process [6], which could be used to obtain a good circular vascular structure. As discussed previously, an important aspect of ink-jet printing in manufacturing technology is the process by which adjacent drops interact to form a linear bio-structure. This methodology, however, produces an irregular deposit with poor surface roughness for each printed layer, with a consequent risk of defects from the poor penetration of the liquid. If printing is conducted with appropriate drop spacing to allow for overlap before solidification, the interaction between adjacent liquid drops and the consequent influence of surface tension will produce smooth surfaces and eliminate possible defects between solidified drops. Fully understanding the spreading characteristics of droplets on the bio-structure and printing multiple overlapping droplets, therefore, are critical for the construction of successful bio-structures.

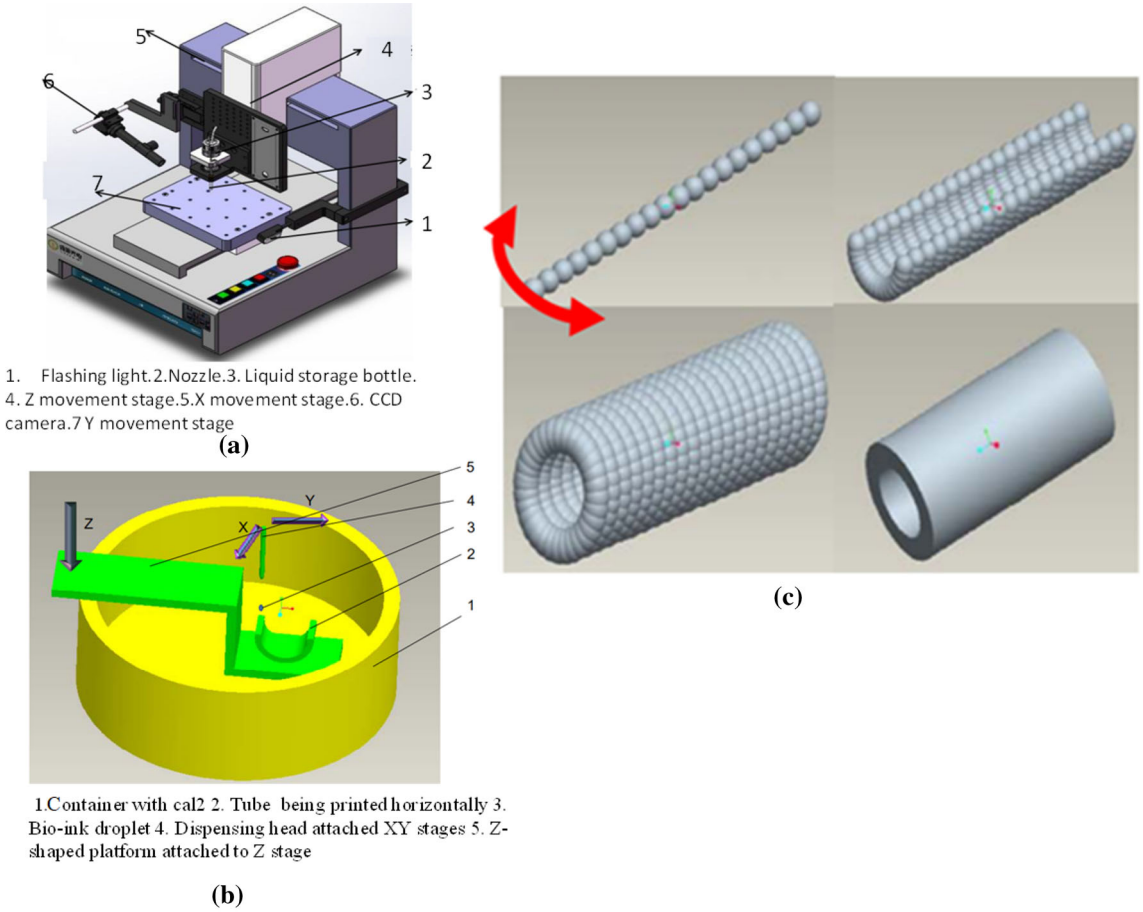

Fig. 1 Typical 3D vascular structure printing process. **a** Print setup, **b** the typical horizontal printing process, **c** multiple droplets overlapping to form a vascular structure

Research background

Challenging problems in the dynamics of drop impact and spreading have existed for many years. The important factors that govern the drop dynamics on a solid surface are the liquid properties (density, surface tension, and viscosity), the surface characteristics (contact angle and roughness), the drop impact velocity, and the surface inclination [7].

In experimental research, Duineveld et al. studied the stability of ink-jet-printed liquid lines and constructed a model to illustrate the dynamic instability that occurs due to a newly arrived drop. They found that when given a sufficiently small transport flow rate, the printed line should be stable, and the width of the printed line should be constant [8]. Sikaloet et al. used high-speed cameras to determine how different viscous droplets affect the deformation of paraffin and glass panels at different impact velocities. Their research results revealed that viscosity affects the spreading process of droplets [9, 10]. Roux et al. studied the spreading characteristics of droplet impact walls under different collision speeds. They pointed out the linear relationship between the velocity of the three-phase contact line and the velocity of impact and found that the impact of droplets could not be fully understood by energy conservation [11].

In theoretical research, Bennett et al. derived the maximum spreading radius of a droplet hitting a plate from the viewpoint of energy conservation [12, 13]. By analyzing the surface force and gravity of the droplet, Vafaei et al. determined the influence of the size of the droplet on its contact angle [14, 15]. Eggers et al., via the law of conservation of mass and momentum, found that the spread of droplets could be divided into the phases of initial non-viscous spreading, the growth of the boundary layer, the formation of liquid film, the spreading of the liquid film, and the formation and retraction of the liquid film edge. They presented a quantitative discussion of the thickness of the boundary layer and the retraction of the edge of the liquid film [16]. Shamit et al. evaluated the droplet impinging on a drying spherical surface and pointed out that the Reynolds number of droplets and the dimensionless diameter of the surface affect the thickness of the liquid film formed after the impact.

In the numerical simulation research field, Quan used the Boltzmann method to simulate droplet collision. The results demonstrated that the maximum relative diameter of the droplet is linear with the web number [17, 18]. Zeng et al. used VOF to simulate the impact of a single droplet on a solid wall and found that the change of the flow field in the droplet is critical in the change of the droplet shape. Tao et al. analyzed the influences of the droplet radius, viscosity, contact angle, and impact velocity on the maximum spreading radius of droplets by the numerical simulation of the spreading characteristics after droplet collision [19, 20].

Although much research was conducted on droplet impact regarding smooth surfaces, due to the difficulty of droplet molding and the complexity of the problems, there are few experimental studies on the actual process of linear bio-structure formation. This work focuses on printing linear bio-structures, namely vascular tubes. To fabricate vascular tubes using ink-jet printing, several requirements must be satisfied. First, stable bio-ink suspensions with defined fluid properties must be produced such that they can be passed through a droplet generator and form regular drops. Second, these suspensions must be delivered onto a substrate or a previously printed layer of solidified bio-ink, and the drops must be in sufficient proximity to each other to allow them to interact and form the desired linear structure features. Next, the printed bio-ink must undergo a phase transition to a solid deposit. Finally, to produce 3D structures, the deposition and drying processes must be repeated on a layer of pre-deposited and dried material. This work pays more attention to the processes of droplet deposition and fusion, and the optimization of which will aid in the direct printing of vascular tubes. The remainder of the paper is organized as follows. "Mathematical model of a linear bio-structure printing process" section provides a mathematical model of droplet deposition and fusion processes. "Simulation analysis of the droplet deposition process and linear bio-structure formation process" section presents the numerical simulation of droplet impacting processes and droplet coalescence simulation and the conditions and results of an experiment of linear bio-structure printing. "Conclusion" section concludes the paper.

Mathematical model of a linear bio-structure printing process

Figure 2 summarizes the typical series of printing processes of ink-jet printing events described so far and includes typical droplet impacting and a succession of droplets overlapping to form a structure. The droplet falls on the solid substrate with certain conditions. Under the combined action of the inertial force, surface tension, and viscous force, the droplet will continue to spread and retract on the solid surface, as illustrated in Fig. 2a. Under the action of viscous dissipation, the amplitude of this state will become increasingly smaller, and finally, the droplet will remain on the base; this is called a static spread. Then, a fluid structure such as a linear structure (Fig. 2b) is formed by printing a succession of overlapping droplets. The typical mathematical model, therefore, includes two parts: (1) a single-droplet spreading process model and (2) a multiple-droplet overlapping process model.

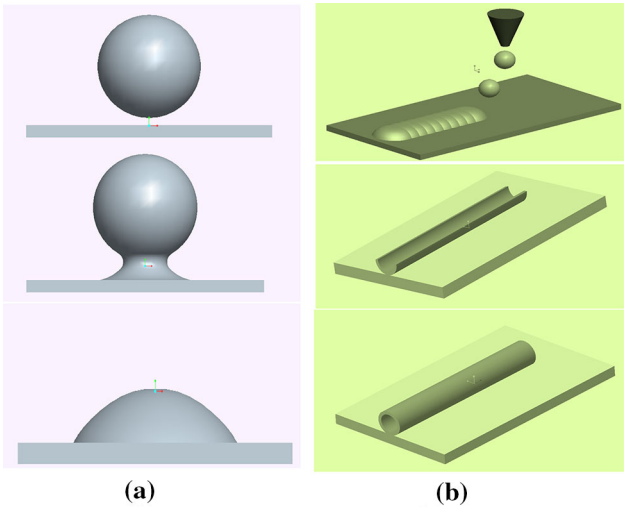

Fig. 2 Typical 3D bio-printing processes. **a** A single-droplet spreading process, **b** multiple droplets overlapping to form a linear structure

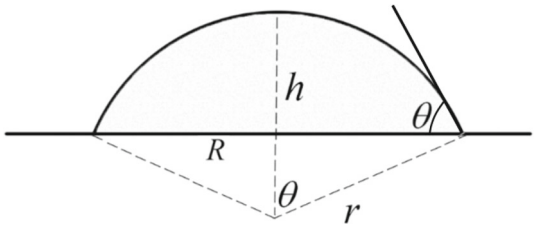

Fig. 3 The model of droplet spreading on a substrate

Droplet spreading process dynamics model

The entire volume of droplets can be kept unchanged during dropping. As shown in Fig. 3, the droplets falling on the substrate are part of a sphere, such as a droplet diffusion cap.

Because the total volume of droplets does not change when dropping, the volume of droplets falling on the substrate should be equal to the spherical volume of droplets in the air. It could be concluded that the spreading coefficient β is:

$$\beta = \frac{R}{R_{\text{droplet}}} = \sin\theta \times \sqrt[3]{\frac{4}{(2+\cos\theta)(1-\cos\theta)^2}}, \quad (1)$$

where R_{droplet} is the radius of the initial droplet, R is the droplet spreading radius, r is the radius of the gap, h is the height of the cap, and θ is the contact angle.

From Eq. (1), the spreading radius of the droplet is related to the contact angle. When the contact angle is fixed, the spreading coefficient is fixed. The theoretical derivation process, however, is under ideal conditions and does not consider viscous dissipation and other problems. In the early stages of droplet diffusion, the kinetic energy is in the dominant position. As the droplet spreads further, kinetic energy is slowly converted into surface energy. Part energy is consumed by the internal flow of the droplet (i.e., viscous dissipation) and by the friction between the droplet and the substrate during diffusion.

The kinetic energy E_{K1} before impact could be represented by Eq. (2):

$$E_{K1} = \left(\frac{1}{2}\rho U_0^2\right)\left(\frac{\pi}{6}D_0^3\right), \tag{2}$$

where U_0, D_0, and ρ are the dropping speed, diameter of the droplet, and density of the fluid, respectively.

The surface energy of the droplet E_{S_1} can be written as Eq. (3):

$$E_{S_1} = \pi D_0^2 \sigma, \tag{3}$$

where σ is the surface tension.

Equation (4) gives the surface energy of droplets falling on the substrate and spreading to the maximum area:

$$E_{S_2} = \frac{\pi}{4} D_{\max}^2 \sigma (1 - \cos\theta_a), \tag{4}$$

where θ_a is the contact angle when spreading to the maximum area.

The viscous dissipated energy W could be expressed as Eq. (5):

$$W = \int_0^{t_c} \int_{\Omega} \phi \mathrm{d}\Omega \mathrm{d}t \approx \phi \Omega t_c, \tag{5}$$

where t_c is the spreading time, Ω is the volume of the viscous fluid, and ϕ is the dissipation function. The thickness of the spreading boundary layer δ could be expressed as Eq. (6):

$$\delta = \frac{2D_0}{\sqrt{Re}}, \tag{6}$$

where Re is the Reynolds number of the fluid. The flow of spherical droplets impacting on the substrate at the initial velocity is equal to the volume spread on the substrate, so it can be concluded that:

$$\frac{U_R}{U_0} = \frac{d^2}{4Dh}, \tag{7}$$

where U_R is the droplet spreading speed, d is the spreading diameter of the base plate when the droplet impacts approximately half of the original diameter of the droplet, D is the diameter of the wetted surface area, and h is the thickness of the liquid when spreading to the maximum diameter. h could be represented as Eq. (8):

$$h = \frac{2D_0^3}{3D_{\max}^2}. \tag{8}$$

The lost energy during the dissipation process can be estimated by Eq. (9):

$$W = \frac{\pi}{3}\rho U_0^2 D_0 D_{\max}^2 \frac{1}{\sqrt{Re}}. \tag{9}$$

According to the principle of the conservation of energy, a new spread factor computation formula can be obtained as Eq. (10):

$$\beta_{\text{new}} = \frac{R}{R_{\text{droplet}}} = \sqrt{\frac{We + 12}{3(1 - \cos\theta) + 4(We/\sqrt{Re})}}. \tag{10}$$

In "Simulation analysis of the droplet deposition process and linear bio-structure formation process" section, the accuracy of the predictions using Eq. (10) is evaluated by comparing the results of experimental measurements for a variety of droplet-surface combinations.

Droplet overlap model

When the nozzle accelerates and reaches the target position corresponding to the observation point, the programmed printing sequence starts. Encoder feedback is used to send the main hardware trigger to the waveform generator to start the pulse at a controlled frequency. The transmission frequency f is combined with the nozzle moving speed v to determine the center distance between the prints of Δx.

$$\Delta x = \frac{v}{f} \tag{11}$$

A linear bio-structure with a length of L and several droplets N is expressed as:

$$N = \frac{L}{\Delta x} + 1. \tag{12}$$

The necessary geometric criterion for the continuous printing of droplets under a given condition is that the distance between the droplets must be less than two times the equilibrium wetting radius r_e of a single droplet on the surface of the substrate, namely

$$\Delta x < 2r_e. \tag{13}$$

This is not a satisfactory condition, because the original droplet on the surface could shrink to a wetting radius smaller than that of r_e before the next small drop of liquid. The effect on the droplet is the surface of a fixed droplet with a balanced contact angle of θ on the substrate. If Δx is large enough, a

single fixed droplet will be formed. The overlap of droplets could be expressed as:

$$f\left(2R_{\text{droplet}}\right)/U > v(\theta), \tag{14}$$

where U is the moving speed of the base plate,

$$v(\theta) = \left[\frac{\sin^3\theta}{4}(1-\cos\theta)^2(2+\cos\theta)\right]^{\frac{1}{3}} \quad \theta < \frac{\pi}{2}, \tag{15}$$

$$v(\theta) = \left[\frac{1}{4}(1-\cos\theta)^2(2+\cos\theta)\right]^{\frac{1}{3}} \quad \theta > \frac{\pi}{2}. \tag{16}$$

When the equation is satisfied, the overlapping droplets converge and form a continuous linear structure. The shape of the linear bio-structure is controlled by the contact angle on the smooth substrate. Here, a model is proposed based on the contact angle θ, which defines the contact width between the droplet and substrate b, and the maximum width is w_f; which is expressed as:

$$\frac{b}{2R_{\text{droplet}}} = \sqrt{\frac{2\pi\sin^2\theta}{3(\theta-\sin\theta\cos\theta)}\cdot\frac{f\left(2R_{\text{droplet}}\right)}{U}}, \tag{17}$$

$$\frac{W_f}{2R_{\text{droplet}}} = \sqrt{\frac{2\pi\sin^2\theta}{3(\theta-\sin\theta\cos\theta)}\cdot\frac{f\left(2R_{\text{droplet}}\right)}{U}} \quad \theta < \frac{\pi}{2}, \tag{18}$$

$$\frac{W_f}{2R_{\text{droplet}}} = \sqrt{\frac{2\pi}{3(\theta-\sin\theta\cos\theta)}\cdot\frac{f\left(2R_{\text{droplet}}\right)}{U}} \quad \theta > \frac{\pi}{2}. \tag{19}$$

This can be derived from geometric considerations. It can then be extended to the wetting condition of a balanced linear bio-structure. The theoretical derivation provides a theoretical basis for the study of the spreading radius of the droplets.

Simulation analysis of the droplet deposition process and linear bio-structure formation process

Single-droplet impact on the substrate

During droplet ejection, the droplet striking the plate surface is a typical gas–liquid, two-phase flow problem. The key is to track the free surface, namely the droplet contact with the air medium. The changes of the related parameters could also be calculated directly in the simulation model. The droplet deposition simulation model proposed in this paper has the following assumptions:

1. The fluid diffusion process is an incompressible Newtonian fluid.
2. The droplet spray liquid is stable, and its properties will not change with time or position.
3. All structures and fluids are centered on the central axis.

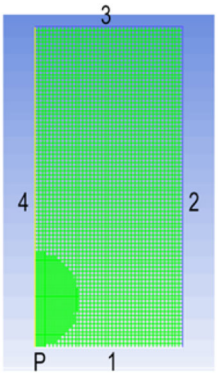

Fig. 4 Boundary definition of grid partition

Because spreading after droplet collision is a symmetric process, an axisymmetric model is adopted to reduce the computational complexity and shorten the computation time. To reduce the solution time, the model does not involve the droplet formation process. A spherical droplet with an initial velocity is defined in the model.

The properties of the fluid are determined by phase separation in the control volume. In this study, the air is set as the main phase, the droplet is set as the second phase, and the volume fraction of the droplet is used to track the material type. The spreading behavior of the droplets is determined by the interaction of the inertial force, the viscous force, and the surface tension. There are many dependent factors during the spreading process during which droplets could rebound or even break, and the process of deformation differs from case to case.

In Fig. 4, interface 1 is defined as the nonslip wall, interfaces 2 and 3 are defined as the pressure inlet, and interface 4 is defined as the symmetry axis. In this case, the surface tension of the liquid is 0.073 N/m, the dynamic viscosity is 20 cp, the density is 1150 kg/m^3, the radius of the droplet is 80 μm, the initial velocity of the droplet is 2 m/s, and the operation time is set to 500 μs. Figure 5 presents a simulation of droplets impacting the substrate at a certain speed and then spreading on the substrate.

As presented in Fig. 5, the entire process can be divided into three main stages. The first stage is the spreading stage, which occurs between 0 and 100 μs. The droplets, which are rapidly deformed after contacting the substrate, extend along the horizontal direction of the substrate to the maximum transverse radius. The second stage is the relaxation stage, which occurs between 100 and 350 μs. The direction of the liquid surface is finally extended after the slow expansion is stopped. The droplet film gradually increases and slowly begins to reverse until the radius gradually trends to a stable value. The third stage is the wetting equilibrium stage, which occurs after 350 μs, and at the end of the droplet

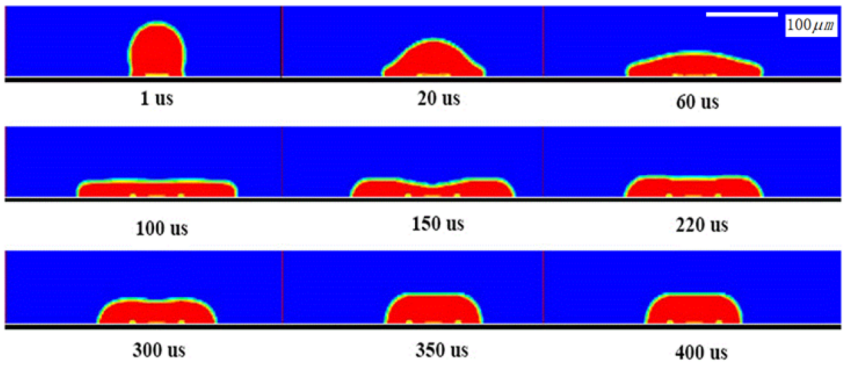

Fig. 5 Simulation of a single-droplet spreading process

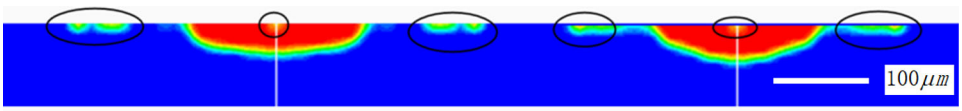

Fig. 6 Bubbles involved during the spreading process

energy dissipation, a stable liquid film is formed. When the expansion period is short, the spherical droplet drastically deforms in a short time, and a flat film is formed on the surface of the substrate.

The second stage lasts longer, but the corresponding morphological changes are not as strong as those during the first stage and are eventually stabilized. The free surface of the liquid film presents an automatic contraction trend due to surface tension where the angle between the cutting edge and the substrate is the contact angle. During the process of droplet impact, the introduction of bubbles is inevitable. The bubbles in the core part of the image are difficult to discharge, and holes will form when the droplets evaporate, which is not conducive to the continuity of the final film formation.

The essence of droplet spreading is the two-phase change of liquid to gas. The liquid phase is replaced by the gas phase, so when the liquid has viscosity, part of the gas is involved in the liquid when the velocity is not synchronized during the dynamic contact process. As presented in Fig. 6, there are bubbles in the center of the droplet, and bubbles on both sides of the droplet are found to escape during simulation.

Influence of the contact angle on the spread of droplets

To study the spreading of droplets at different contact angles, 12 groups of parameters are set to simulate the contact angle from 10 to 120 degrees. The surface tension of the material is 0.073 N/m, the dynamic viscosity is 20 cp, the density is 1150 kg/m^3, the droplet diameter is 80 μm, and the droplet dropping speed is set to 1 m/s. A running time of 500 μs is set to simulate the spreading of different contact angles. The droplet spreading radius varies with time, as shown in Fig. 7. When the time is close to 120 μs, the radius reaches the maximum. After that time, the droplet begins to contract, and the radius becomes small.

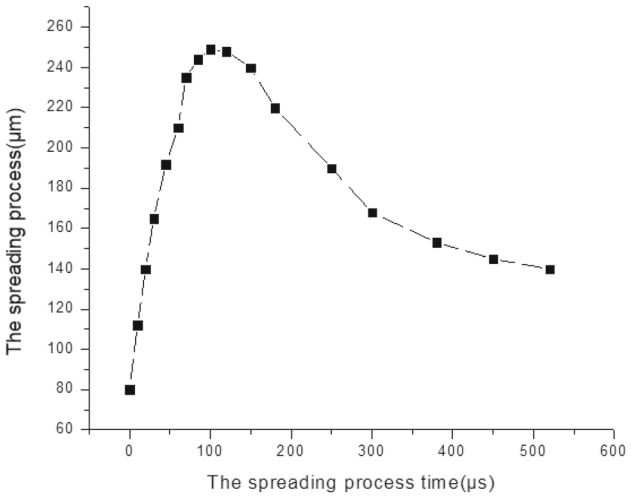

Fig. 7 Change of the spreading radius of a liquid drop

Figure 8 presents the entire spreading process of the droplet. The following can be concluded: (1) The larger the contact angle, the larger the maximum droplet spreading radius. The spreading radius will first increase and then decrease. (2) The greater the contact angle, the faster the deformation process, and the shorter the time for the droplet to reach equilibrium. (3) The larger the contact angle, the smaller the droplet radius, and the thicker the film.

Influence of velocity on the spread of droplets

The droplets on the base affect the effect of droplet spreading on the base of the substrate. In this simulation, a suitable 60-degree contact angle is selected as the basic parameter, the surface tension of the material is 0.073 N/m, the dynamic viscosity is 20 cp, the density is 1150 kg/m^3, and the diameter of the droplet is 80 μm. To spread the droplets successfully, independent droplets must be generated. A single droplet is

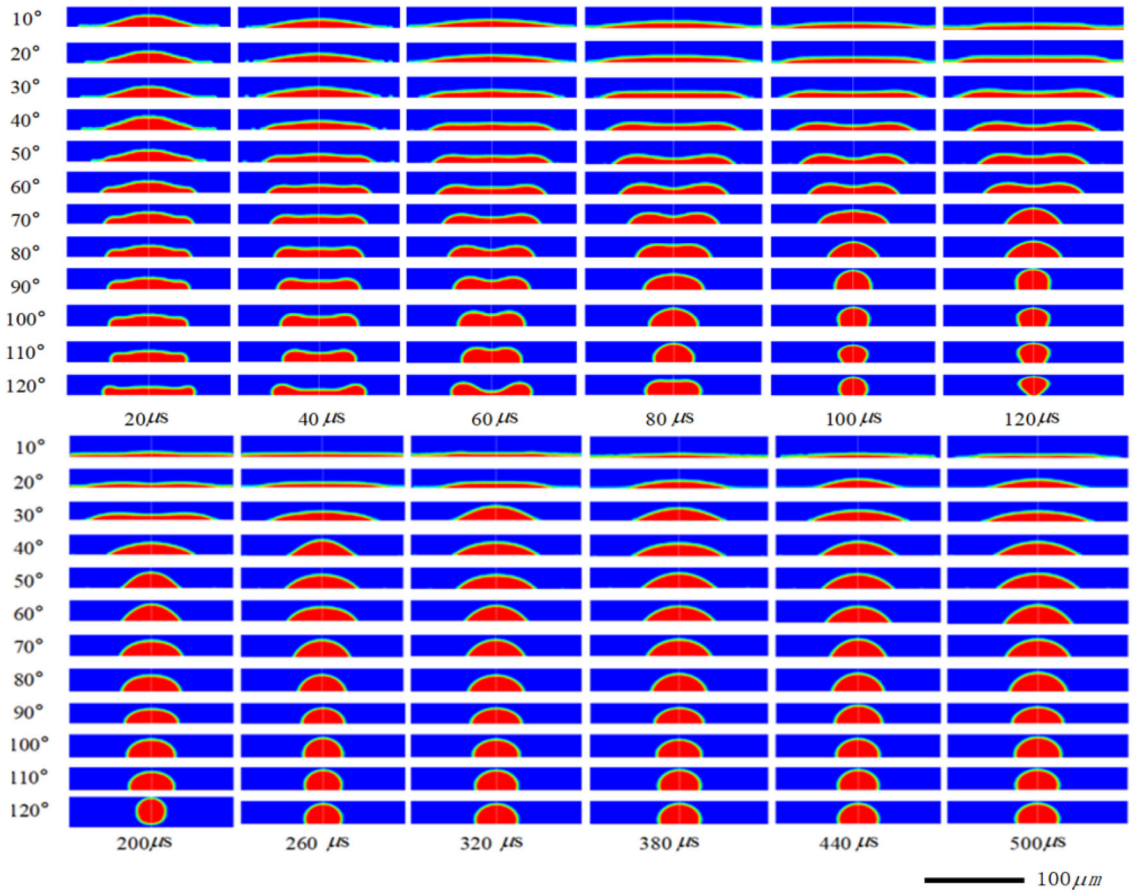

Fig. 8 Change diagram of the volume fractions of different contact angles

generated under the coordination of certain voltage parameters and pulse width. Scholars have conducted relevant, in-depth research on the formation and speed of droplets, which were determined to be between 0.5 and 5 m/s [21, 22]. In this study, the initial velocities of the droplets that are spread on the substrate, therefore, are set to 0.8, 1.2, 1.5, 1.8, 2.1, and 2.5 m/s, and the running time is set to 500 μs. Figure 9 shows the change process of the droplet morphology.

The following can be concluded from Fig. 9: (1) With the increase in velocity, the maximum spreading radius of the droplet will gradually increase; however, if the velocity is too large, the droplet will break down into a stable deposition; (2) The initial velocity of the droplet has little effect on the radius of the droplet balance if the velocity is too fast, because the viscosity is not enough to lead to the liquid. The droplets are separated into scattered shapes. (3) The larger the initial velocity of the droplets, the faster the deformation rate, and the longer the equilibrium time.

Droplet spreading, therefore, is a complicated process. The spreading of droplets under different conditions was investigated in this section. The changes in internal velocity at different times of droplet spreading are further analyzed, as presented in Fig. 10.

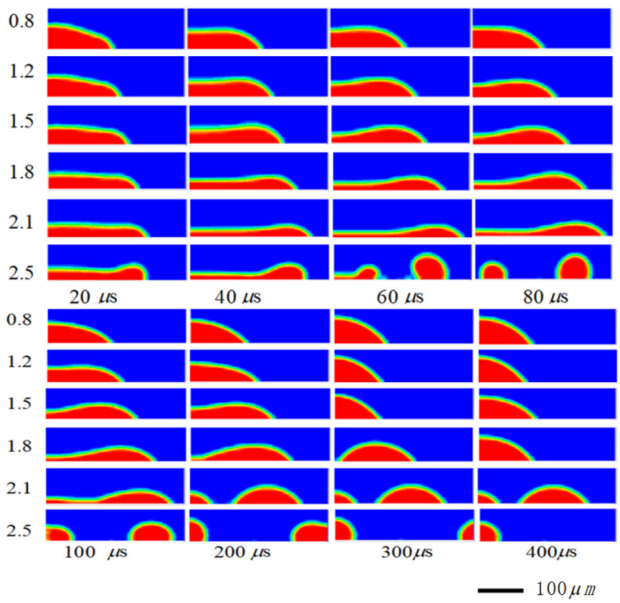

Fig. 9 Change diagram of the volume fraction of droplets at different speeds

The velocity vector diagrams at different times presented in Fig. 10 reveal the flow trend of the droplets at different

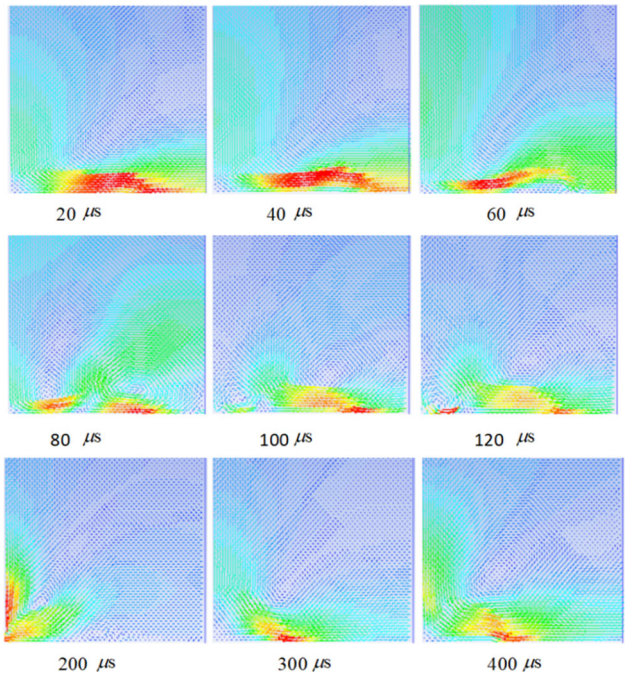

Fig. 10 The velocity vector clouds during the spreading process

times during the entire process. During the process of droplet spreading, the droplet has a velocity of outward flow and an upward movement trend in the center of the droplet. When the time reaches 120 μs, the droplet is close to the equilibrium state. The flow fluctuates, moves downward for a moment, and then moves upwards; the droplet will oscillate at this stage and eventually reach the equilibrium state.

Simulation of multiple-droplet depositions to form a linear bio-structure

In this section, a two-droplet fusion simulation process is reported to research continuous, multiple-droplet depositions. The nozzle used in the simulation has a 10 μs average jet velocity v_{droplet} of the convex surface. The nozzle is defined as having a base total height of H, and two under the emission frequency of the nozzle. The height difference between droplets could be expressed as Eq. (20):

$$H = \frac{v_{\text{droplet}}}{f}. \tag{20}$$

The other parameters remain unchanged, and the numerical simulation is conducted in the case of a 60-degree contact angle with an initial velocity of 1.5 m/s, a center height difference of the drop of 80 μm, and an interval of 180 μm. Figure 11 presents the simulation results of the two-droplet fusion process.

The simulation analysis reveals that the droplets are well separated at the appropriate contact angle, initial velocity, height difference, and proper interval, the surface morphology is better, and the thickness of the film is suitable.

Experiment of the linear bio-structure printing process

To investigate the drop formation dynamics and identify the optimum printing parameters, a DoD ink-jet printing system was setup, as depicted in Fig. 12. The DoD stimulation pulse was produced by a MicroFab Jet Drive. A pneumatic regulator was used to regulate the backpressure of the solution tank's dispensing head to obtain a perfect meniscus for a fine droplet. Throughout the experimental period, the backpressure was adjusted within the range of 3.0–1.2 kPa to aid the droplet development. An electrical energy waveform (voltage waveform) was used as external stimulation to make the PZT instrument deflect circularly. This deformation transformed into pressure pulses and was applied to the solution inside the nozzle. In general, each stimulation phase is accountable for printing droplets in DoD ink-jetting.

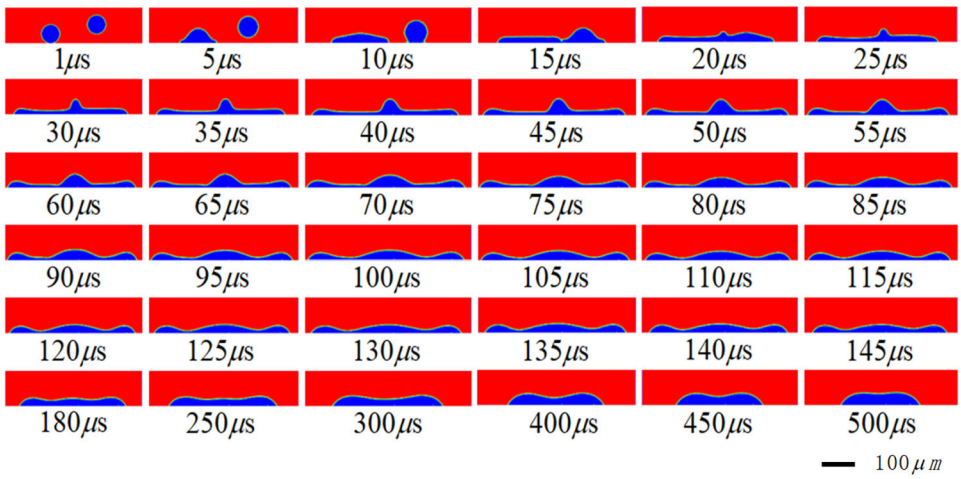

Fig. 11 Spreading and fusion simulation of two continuous droplets

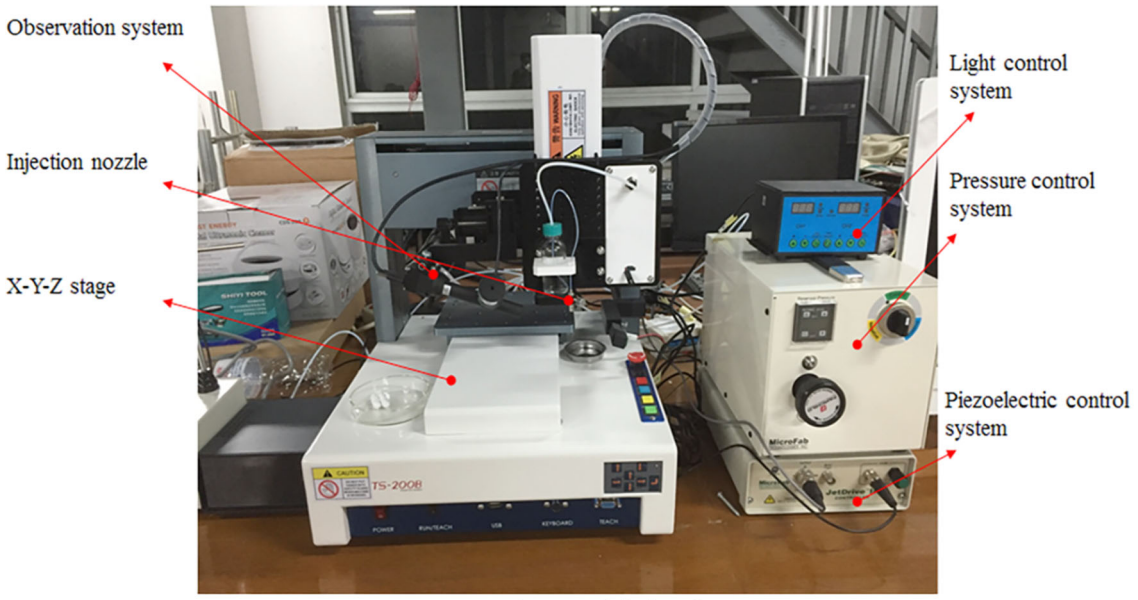

Fig. 12 Experimental ink-jet setup

Fig. 13 Single-droplet spreading process observation

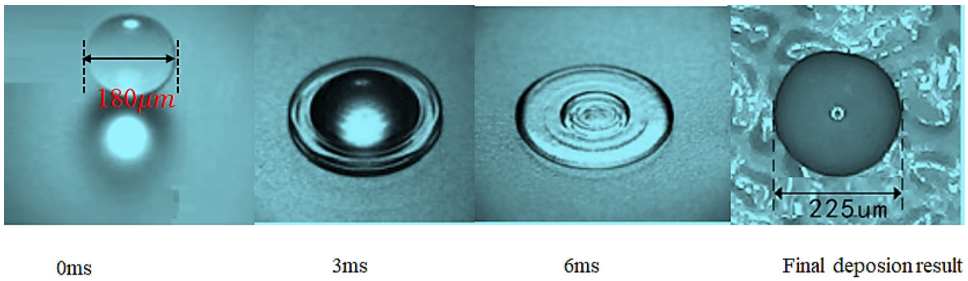

A 0.3% concentration of sodium alginate water solution was selected for experimentation. The physical parameters of the solution were similar to those used in the numerical simulation. The contact angle of the solution and the printed substrate was about 60 degrees as the instrument began to pulse at the controlled frequency, which was determined by the joint action of the emission frequency f and the moving speed v of the shot head. The center of the printed drops was Δx. The spread of the droplets can also be changed by the trigger frequency and the contact angle. The initial speed and the time interval of the droplets can be controlled with different printing effects. Figure 13 depicts the single-droplet spreading process of a drop on a substrate obtained by a vertical electronic magnifying mirror during the actual process. Before the droplet was dropped on the surface, a whole fluid sphere with a diameter of 180 μm was observed. The droplet underwent spreading when the time was 3 ms. The spreading process finished close to 6 ms, and the final spreading diameter was about 225 μm.

The deposition radius of the droplets can be solved accurately via simulation, and the distance between the droplets, therefore, can be controlled by only controlling the moving speed of the nozzle and the trigger frequency of the droplet. The velocity of the droplet is changed by the voltage amplitude of the piezoceramic to obtain different printing paths. Figure 14a–d presents the deposition conditions under the printing frequencies of 70, 90, 110, and 150 Hz.

When the droplet spacing is less than the spreading diameter of the droplets, the droplets cannot be connected, as shown in Fig. 14a. When the droplet spacing is close to the deposition diameter, slight fusion will occur between them, as shown in Fig. 14b. When the distance between the droplets is about 80% of the droplet spreading radius, the effect of the deposited line segment is better, and the droplet spacing is about 50% of the droplet spreading radius, as shown in Fig. 14c and d. When the overlap rate is high, the deposition result is a straight line, the width of which is wider than the spreading diameter of the droplet, affecting the printing accuracy.

Experiment of the bio-ink printing process

Two processes occur during the printing of bio-ink with cells: the formation and spraying of cell droplets and the

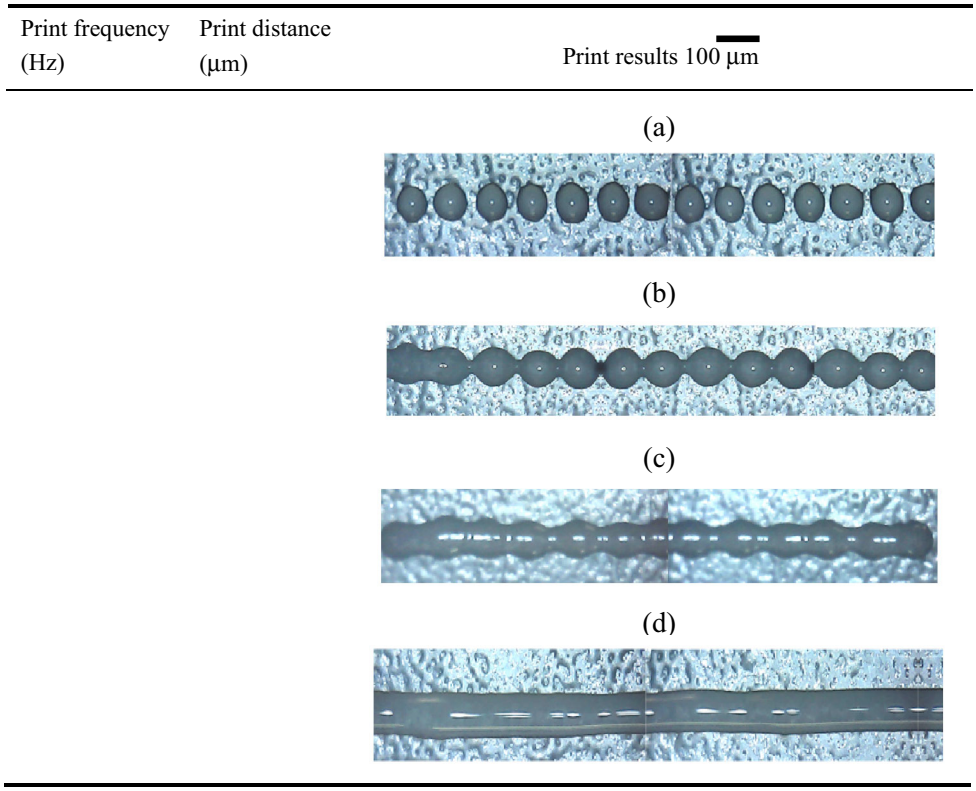

Fig. 14 Linear structure printing results under different parameters

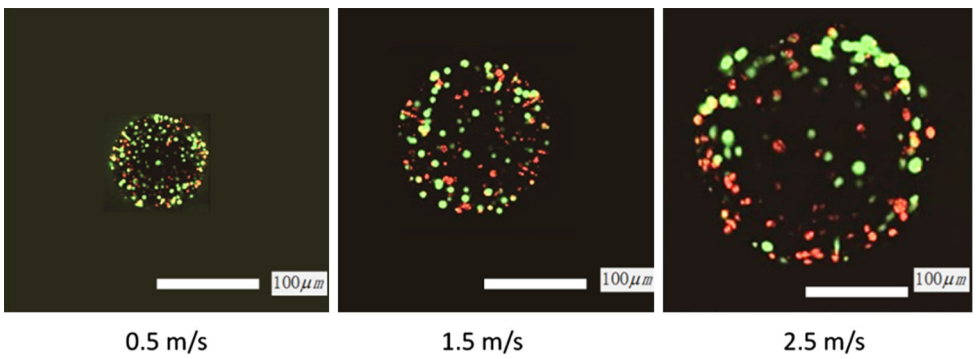

Fig. 15 Bio-ink droplet spreading process at different injection speeds (red cells are dead cells and green cells are live cells)

landing of cell droplets, both of which could cause cell damage. During the process of cell droplet landing, the sprayed cell droplet lands on the receiving substrate at a certain vertical speed. After a period of decline, the cell collides either once or repeatedly with the receiving substrate, and the cell suffers mechanical damage. The bio-ink used in this experiment was composed of cells surrounded by hydrogels. After continuous injection, the first droplets of the injected cells first entered the gel coating area and collided with the hydrogel, and the latter droplets were sprayed down as per the set print interval. The two cell droplets will collide and melt in the hydrogel coating. It, therefore, is necessary to study cell death before and after spraying. The experimental conditions were as follows. The bio-ink was composed of 0.3% sodium alginate solution and 293T cells. Sodium alginate is used as a typical hydrogel for cell encapsulation in medical and biomedical engineering.

Among various biomaterials for the encapsulation of biomaterials, alginate hydrogel attracted much attention due to its great similarity to a natural extracellular matrix (ECM) and its ability to serve as a cellular immune barrier. Sodium alginate is a type of natural polysaccharide polymer extracted from seaweed, which has a high molecular weight, linear shape, and high hydration. Its water-soluble salts, therefore, have a high viscosity at low concentrations, making it a good thickening and suspending agent. Its molecular chain contains several hydroxyl and carboxyl groups. Under the condition of two valence ions, such as Ca2+, cross-linked calcium alginate polymers will form, showing that the gel state with high water content is ridiculed [23]. The nozzle adopted for the experiment was a 120-micron-diameter MJ-ABL-01

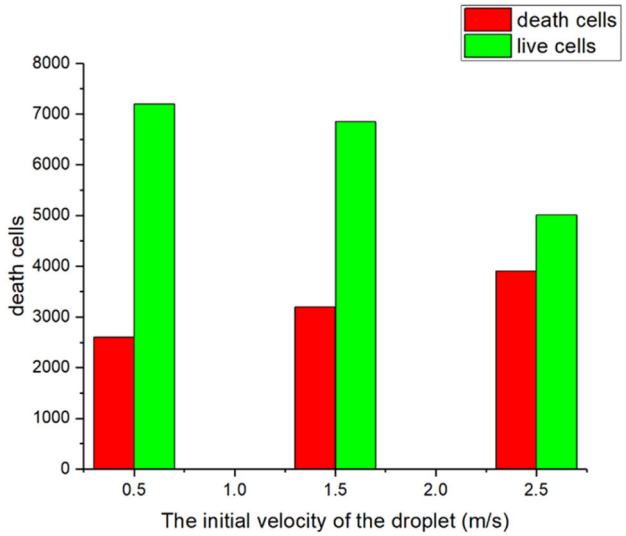

Fig. 16 The dead and live cells in the droplets at different initial injecting speeds

MicroFab nozzle, which was controlled by different pressures to obtain different spraying speeds. In this study, cell death and life statistics were obtained under the conditions of initial velocities of 0.5, 1.5, and 2.5 m/s. It was found that the spreading diameter of a single cell droplet was circular with different velocities and diameters. As depicted in Fig. 15, when the velocity was 0.5 m/s, the spreading diameter was about 135 μm. When the velocity was 1.5 m/s, the spreading diameter was about 160 μm. When the velocity was increased to 2.5 m/s, the spreading diameter reached about 210 μm. With the increase in the printing speed, the number of dead cells also increased. The reason for cell death was that the cell suspension died during the process of droplet formation and collision with the substrate, as presented in Fig. 16.

Conclusion

By establishing a mathematical equation of a spherical droplet model, the researchers could determine the simple relationship between the static spreading of the droplet, the velocity of the droplet, and the contact angle. The influences of various parameters on the static spreading of the droplets were studied. Experimental observation of the common spread of several droplets was made according to these analyses. The following conclusions were obtained.

1. The simple theoretical formula of the static spreading of droplets can be used to analyze the static spreading of droplets on a flat surface, as well as the change laws of the droplet velocity and contact angle.
2. Calculation by the theoretical model agreed with the results of numerical simulations and actual experimentation in the range of all simulated contact angles and velocities. Furthermore, the variation laws were the same, and the errors were small.
3. The influence laws of droplet spreading determined in this work are as follows. (a) The greater the velocity, the greater the maximum spreading radius of the droplet; however, if the velocity is too large, the droplet will break down to a stable deposition. (b) The size of the initial velocity of the droplet has little effect on the radius of the droplet balance. When the velocity is too fast, because the viscosity is not enough to lead to droplet formation, it is separated into a scattered shape. (c) The greater the initial velocity of droplets, the faster the deformation rate, and the longer the equilibrium time. (d) When the contact angle is larger, the maximum spreading radius of the droplet first becomes larger and then smaller. (e) The greater the contact angle, the faster the deformation process, and the shorter the time it takes for the liquid drop to reach equilibrium.
4. It has been demonstrated that bio-ink drops could form stable lines through the coalescence of trains of overlapping drops with proper printing parameters. By increasing the printing speed, the spreading diameters become bigger, and the number of dead cells increases. To achieve a better cell printing survival rate, it is critical to adjust the printing speed and the thickness selection of the gel layer on the substrate. In future research, the optimum printing parameters should be investigated to obtain a good survival rate of cells.

The results of this paper provide a solid theoretical basis for the subsequent implementation of the 3D assembly of complex biological structures using micro-droplet injection technology.

Author contributions Conceptualization, Youping Gong and Xiangjuan Bian; Data curation, Zhikai Bi, Jingyang He, and Guojin Chen; Formal analysis, Youping Gong, Xiangjuan Bian and Xiang Zhang; Funding acquisition, Youping Gong, Huifeng Shao and Guojin Chen; Investigation, Jingyang He; Methodology, Youping Gong, Xiangjuan Bian; Project administration, Youping Gong; Resources, Anlei Ge; Software, Youping Gong, Zhikai Bi, Wenxin Li and Jingang He; Supervision, Youping Gong; Validation, Xiangjuan Bian; Writing – original draft, Youping Gong, Zhikai Bi, Xiangjuan Bian and Anlei Ge; Writing – review & editing, Xiangjiuan Bian.

Funding The work is financially supported by the National Natural Science Foundation of China (51805475, 51675148)

Compliance with ethical standards

Conflict of interest The authors declare no conflicts of interest.

Ethical approval This study does not contain any studies with human or animal subjects performed any of the authors.

References

1. Murphy SV, Atala A (2014) 3D bioprinting of tissues and organs. Nat Biotechnol 32(8):773–785
2. Hölzl K, Lin S, Tytgat L, Vlierberghe SV, Ovsianikov A (2016) Bioink properties before, during and after 3D bioprinting. Biofabrication 8(3):032002
3. Jin Y, He Y, Gao Q et al (2014) Droplet deviation modeling and compensation scheme of inkjet printing [J]. Int J Adv Manuf Technol 75(9):1405–1415
4. Zhang M, Krishnamoorthy S, Song H et al (2017) Ligament flow during drop-on-demand inkjet printing of bioink containing living cells. J Appl Phys 121:124904
5. Xu C et al (2012) Scaffold-free inkjet printing of three-dimensional zigzag cellular tubes. Biotechnol Bioeng 109:3152–3160
6. Gong Y, Lv Y, Su S et al (2016) The predictive compensation path research of the micro tube fabrication process. Microsyst Technol 22:2209–2222
7. Lunkad SF, Buwa VV, Nigam KDP (2007) Numerical simulations of drop impact and spreading on horizontal and inclined surfaces [J]. Chem Eng Sci 62(24):7214–7224
8. Duineveld PC (2003) The stability of ink-jet printed lines of liquid with zero receding contact angle on a homogeneous substrate. J Fluid Mech 477:175–200
9. Pasandideh-Fard M, Chen P, Mostaghimi J et al (1996) The generalized Laplace equation of capillarity I. Thermodynamic and hydrostatic considerations of the fundamental equation for interface. Adv Colloid Interface Sci 63:151–177
10. Sikalo S, Tropea C, Ganic EN (2005) Dynamic wetting angle of a spreading droplet. Exp Therm Fluid Sci 29:795–802
11. Sikalo S, Ganic EN (2006) Phenomena of droplet-surface interactions. Exp Therm Fluid Sci 31:97–110
12. Roux DCD, Cooper-White JJ (2004) Dynamics of water spreading on a glass surface. J Colloid Interface Sci 277:424–436
13. Bennett T, Poulikakos D (1993) Splat-quench solidification: estimating the maximum spreading of a droplet impacting a solid surface. J Mater Sci 28:963–970
14. Chandra S, Avedisian CT (1991) On the collision of a droplet with a solid surface. In: Proceedings of mathematical and physical sciences, vol 6, pp 13–14
15. Vafaei S, Podowski MZ (2005) Analysis of the relationship between liquid droplet size and contact angle. Adv Colloid Interface Sci 113:133–146
16. Vafaei S, Podowski MZ (2005) Theoretical analysis on the effect of liquid droplet geometry on contact angle. Nucl Eng Des 235:1293–1301
17. Eggers J, Fontelos MA, Josserand C et al (2010) Drop dynamics after impact on a solid wall: theory and simulations. Phys Fluids 22:062101
18. Bakshi S, Roisman IV, Tropea C (2007) Investigations on the impact of a drop onto a small spherical target. Phys Fluids 19:032102
19. Shenglin Q, Shuang L, Weizhong L et al (2009) A simulation of impact of droplets on solid surfaces by using the lattice Boltzmann method. Chin J Comput Mech 26:627–632
20. Zeng X, Yang F, Qi L et al (2007) Simulation of the shape and flow field of a droplet after impacting a substrate. J Northwest Polytech Univ 25:528–532
21. Xu C, Zhang M, Huang Y et al (2014) Study of droplet formation process during drop-on-demand inkjetting of living cell-laden bioink [J]. Langmuir 30(30):9130–9138
22. Reis N, Ainsley C, Derby B (2005) Ink-jet delivery of particle suspensions by piezoelectric droplet ejectors. J Appl Phys 97(9):815
23. Gao Q, He Y, Fu J et al (2015) Fabrication of shape controllable alginate microparticles based on drop-on-demand jetting [J]. J Sol-Gel Sci Technol 77(3):610–619